

Phase Transformations and Photoluminescence Features of $\text{Gd}_{2(1-x)}\text{Tb}_x\text{Eu}_x\text{O}_3$ Solid Solutions

V. V. Bakovets^{a,*}, I. P. Dolgovesova^a, T. D. Pivovarova^a, and M. I. Rakhmanova^a

^a Nikolaev Institute of Inorganic Chemistry, Siberian Branch, Russian Academy of Sciences, Novosibirsk, Russia

*e-mail: becambe@niic.nsc.ru

Received July 29, 2020; revised July 29, 2020; accepted July 30, 2020

Abstract—Solid solutions $\text{Gd}_{2(1-x)}\text{Tb}_x\text{Eu}_x\text{O}_3$ (where $x = 1$ and 2.5 mol %) are prepared by the sol–gel method with subsequent annealing at 700–1200°C in air and hydrogen atmospheres. It is found by XRD and IR spectroscopy that the solutions undergo the chemical and phase transformations from the cubic modification to the monoclinic one in the annealing process and change the degree of crystallinity. Microinclusions of the $\text{Tb}_7\text{O}_{12}:\text{Eu}^{3+}$ phase are present in a solid solution under certain annealing conditions, which are not formed in a hydrogen atmosphere or with a high activator concentration of 2.5 mol % at 1200°C. In accordance with these transformations, the Tb^{3+} and Eu^{3+} photoluminescence activators are redistributed over the C_{3i} centrosymmetric and C_2 noncentrosymmetric crystal lattice sites and the C_s surface states. These rearrangements give rise to changes in the parameters of the photoluminescence spectra, which are associated with a change in the ways of transferring the excitation energy of the main radiative transitions of the Tb^{3+} and Eu^{3+} photoluminescence activators.

Keywords: solid solutions of rare earth oxides, Tb^{3+} and Eu^{3+} photoluminescence activators, photoluminescence, IR spectroscopy, X-ray diffraction phase analysis

DOI: 10.1134/S1063783420120057

1. INTRODUCTION

Owing to the structural stability, sesquioxides of Y and Gd are excellent matrices for creating phosphors with various emission spectra when doped with photoluminescence (PL) activators based on rare earth elements (REE). The easily accessible and relatively cheap Eu^{3+} and Tb^{3+} activators are widely used REE activators, which make it possible to obtain efficient, strong, and single-center emission in the red (mean wavelength 612 nm), green (542 nm), and blue (487 nm) regions of the visible spectrum [1–4]. These colors are close to the main ones, by mixing of which one can create different shades of the emitted color.

The bixbyite-type lattice, in which cations, including Eu^{3+} and Tb^{3+} , are located in the C_{3i} centrosymmetric and C_2 noncentrosymmetric sites [5–8], is a characteristic feature of the matrices of the cubic modification of $C\text{-Ln}_2\text{O}_3$. For polycrystalline nanoscale powders, the state of activators at the boundaries (surfaces) of crystallites is of particular importance [9, 10]. There are no C_{3i} sites in this state because of distortion of the short-range order of the crystal lattice. The monoclinic modification of $B\text{-Ln}_2\text{O}_3$ sesquioxides is characterized by three different noncentrosymmetric positions of REE elements in the crystal lattice [11–13]. Corresponding changes in

the structure of the first coordination sphere of the PL activator cations, for example, the Eu^{3+} cation surrounded by $(\text{O}^{2-})_6$ ions, lead to redistribution of the excitation energy over radiative electronic transitions and energy losses due to electron–phonon interactions [14–16]. This causes shifts in the maxima of the emission bands and changes in their relative intensities and, finally, in the perception of the color of displays, monitors, and object images. The well-known optical effect of warm–cold lighting can serve as an example of the visual perception of such changes in radiation.

The coexistence of terbium ions with different oxidation states Tb^{3+} and Tb^{4+} is a specific feature of PL compounds with the Tb^{3+} activator. The Tb^{4+} state does not create emission centers. Thus, it is necessary to eliminate the oxidizing atmosphere and use either an inert atmosphere or a vacuum in order to synthesize the corresponding phosphors. Another option requires varying the chemical composition or the lattice structure in order to provide the thermodynamic stability of Tb^{3+} ions at the temperature of the synthesis and under a nonequilibrium oxygen pressure. In connection with the above peculiarities, it must be admitted that a fundamental comprehensive analysis of the chemical composition of the sublattices of Gd, Tb, and Eu cations in the phosphors based on

$\text{Gd}_{2(1-x)}\text{O}_3:\text{Tb}_x\text{Eu}_x$ solid solutions has not yet been carried out from the standpoint of the thermodynamic state of the system, namely, the $\text{Tb}^{3+,4+}$ oxidation state of the cations and the redistribution of the Gd^{3+} , Tb^{3+} (Tb^{4+}), and Eu^{3+} cations in the bixbyite-type lattice and at the boundaries (surfaces) of crystallites. Thus, the objectives of this study were as follows:

—sol–gel synthesis of $\text{Gd}_{2(1-x)}\text{Tb}_x\text{Eu}_x(\text{OH})_y(\text{CO}_3)_z \cdot n\text{H}_2\text{O}$ solid solutions with their subsequent annealing at temperatures of 700, 900, and 1200°C to the corresponding *C*-cubic and *B*-monoclinic modifications of $\text{Gd}_{2(1-x)}\text{O}_3:(\text{Tb}^{3+,4+})_x(\text{Eu}^{3+})_x$ compounds, and characterization of the chemical and structural compositions of the obtained solid solutions;

—analysis of the localization of Eu^{3+} and Tb^{3+} ions over the C_{3i} and C_2 cationic sites and the C_s surface states in the $\text{Gd}_{2(1-x)}\text{O}_3:(\text{Tb}^{3+,4+})_x(\text{Eu}^{3+})_x$ lattice and analysis of the distribution of the emission excitation energy over radiative electronic transitions according to the PL spectra.

2. EXPERIMENTAL

To obtain PL compounds based on $\text{Gd}_{2(1-x)}\text{O}_3:(\text{Tb}^{3+,4+})_x(\text{Eu}^{3+})_x$ solid solutions, we used the sol–gel method [14, 17, 18]. Nitrates $\text{Gd}(\text{NO}_3)_3 \cdot 6\text{H}_2\text{O}$, $\text{Tb}(\text{NO}_3)_3 \cdot 5\text{H}_2\text{O}$, and $\text{Eu}(\text{NO}_3)_3 \cdot 5\text{H}_2\text{O}$ synthesized from the corresponding oxides with at least 99.9% of the main component were used as reagents. The synthesis was carried out starting from aqueous solutions of mixtures of the above salts, the compositions of which corresponded to the ones necessary for the formation of sol–gel products of solid solutions of hydroxocarbonates $\text{Gd}_{2(1-x)}\text{Tb}_x\text{Eu}_x(\text{OH})_y(\text{CO}_3)_z \cdot n(\text{H}_2\text{O})$. For this, 0.2 M solutions of nitrates that corresponded, in percentage, to the compositions of the required oxides were used. A twofold excess of a solution of special-purity grade NaOH in bidistilled water was used a precipitant. The synthesis was carried out on a setup with sputtering of the starting reagents to achieve homogeneity in the volume of the working solution. The resulting precipitate of $\text{Gd}_{2(1-x)}\text{Tb}_x\text{Eu}_x(\text{OH})_y(\text{CO}_3)_z \cdot n\text{H}_2\text{O}$ was washed until neutral pH of the rinsing water was achieved and dried in air at 50°C. The product was divided into parts to form polycrystalline samples weighing 1 g each, which then were annealed at 700, 900, and 1200°C for 1–2 h until formation of the final products, i.e., solid solutions $\text{Gd}_{2(1-x)}\text{O}_3:(\text{Tb}^{3+,4+})_x(\text{Eu}^{3+})_x$, where $x = 1$ and 2.5 mol %. Further, we will use notation $\text{Gd}_2\text{O}_3:\text{Tb}^{3+},\text{Eu}^{3+}$ (x mol %) for brevity. The concentrations of Tb^{3+} and Eu^{3+} were chosen equal to 1 and 2.5 mol %, since the Tb^{3+} and Eu^{3+} ions acquire PL excitation energy independently at Tb^{3+} concentrations of <1.5 mol %, while the Tb^{3+} ions serve as PL coactivators at concentrations of >1.5 mol % and partially

transfer the excitation energy from the 5D_4 level to the 5D_1 of Eu^{3+} cations, for example, in the CaWO_4 matrix [19]. A concentration of 2.5 mol % was found to be the most effective concentration for Eu^{3+} (1–2 mol % in [20, 21]). In [1, 22], it was recommended to use Eu^{3+} concentrations of 1.25 mol % in the Y_2O_3 and Gd_2O_3 matrices for the effective emission of Eu^{3+} cations, but with low concentrations of the Tb^{3+} coactivator at a level of 0.0025–0.0050 mol %. Our goal was to study the distributions of the Eu^{3+} and Tb^{3+} cations over the lattice sites and to analyze the paths of the transfer of the PL excitation energy over the sublattices comprised of the C_{3i} and C_2 sites; therefore, equal concentrations of these ions were chosen.

The X-ray diffraction phase analysis of the samples was performed on a Shimadzu XRD-7000 diffractometer ($\text{CuK}\alpha$ radiation, Ni filter, 2θ range 5°–70°, step 0.03°, and 2s accumulation). IR spectra were recorded on a SCIMITAR FTS 2000 IR spectrometer in the frequency range of 4000–375 cm^{-1} .

The luminescence spectra were studied using a Cary Eclipse fluorescence spectrophotometer (VARIAN). The excitation wavelength was chosen according to the diffuse reflection spectra (DRS) and the excitation luminescence spectra of single vibronic levels (SVL) of the main emission bands of the Tb^{3+} (542 nm) and Eu^{3+} (612 nm) ions. According to preliminary DRS experiments, all polycrystalline samples have a high optical absorbance of about 70–80% in the ultraviolet region. Wavelength $\lambda_{\text{ex}} = 280$ nm was chosen on the basis of the transfer of excitation energy over the maximum possible number of known channels for these compounds, namely, charge transfer channel $\text{Gd}^{3+} \rightarrow \text{Tb}^{3+}$; and electron transfer channels $4f \rightarrow 5d$ Tb^{3+} , 5D_4 (Tb^{3+}) \rightarrow $^5D_{1,2}$ (Eu^{3+}) [2], $4f \rightarrow 4f$ (Eu^{3+}) [1, 19, 22–25], and $\text{O}^{2-} \rightarrow \text{Eu}^{3+}$ [10, 26] for efficient emission of Tb^{3+} and Eu^{3+} ions via the corresponding radiative transitions. In comparison with the cubic modification, the transmittance of the monoclinic modification at a wavelength of $\lambda = 280$ nm was lower by a factor of almost 2, and the excitation efficiency was the same for the band with a maximum at 612 nm and eight times higher for the band with a maximum at 550 nm.

3. RESULTS AND DISCUSSION

Figure 1 shows the X-ray diffraction patterns of the studied samples.

The unit cell parameters of the main phase of *C*- $\text{Gd}_2\text{O}_3:\text{Tb}^{3+},\text{Eu}^{3+}$ (x mol %), the sizes of the coherent scattering regions (CSRs), and accompanying phases are given in Table 1 for the samples obtained by annealing the sol–gel products of $\text{Gd}_{2(1-x)}\text{Tb}_x\text{Eu}_x(\text{OH})_y(\text{CO}_3)_z \cdot n\text{H}_2\text{O}$ under various conditions.

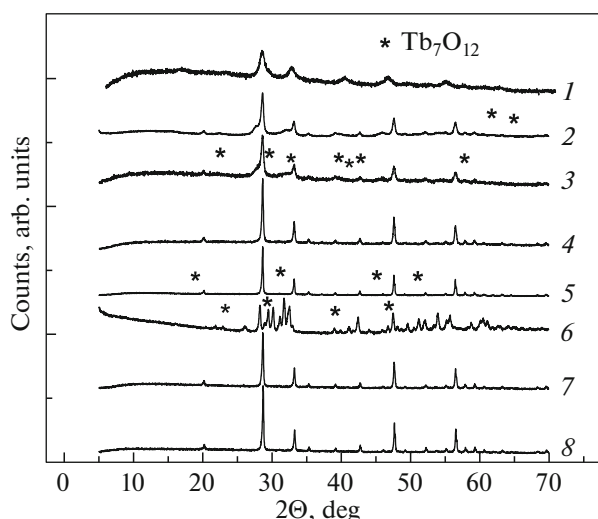


Fig. 1. X-ray diffraction patterns of samples 1–8.

All samples, except for samples 1, 6, and 11, are mainly cubic modifications of $C\text{-Gd}_2\text{O}_3\text{:Tb}^{3+}, \text{Eu}^{3+}$ (x mol %) with the crystal lattice belonging to space group $Ia\bar{3}$. The lattice parameter of sample 5 is closest to that of the Gd_2O_3 matrix. Taking into account the known values of the radii of Eu^{3+} (0.109 nm), Gd^{3+} (0.115 nm), and Tb^{3+} (0.093 nm) ions for a coordination number of 6 in oxides [27, 28], it can be assumed that the Tb^{3+} and Eu^{3+} ions substitute preferably the Gd^{3+} ions of the matrix in the C_{3i} sites, since the volume of the corresponding coordination sphere for the C_{3i} sites is smaller than that for the C_2 sites.

In the X-ray diffraction pattern of sample 1, which is a sol-gel product annealed in air at 700°C for 1 h,

twelve reflections belong to the phase of cubic oxide $C\text{-Gd}_2\text{O}_3$ listed in the Inorganic Crystal Structure Database (ICSD) under entry # 183130 (ICSD-96207), eighteen reflections can be attributed to the $\text{Gd}(\text{OH})_3$ phase (ICSD-152449) in an amount of less than 5 wt %, and eight reflections correspond to the presence of the $\text{Gd}(\text{CO}_3)\text{OH}$ phase (ICSD-200093) at a level of about 1 wt %. The same pattern has been observed earlier [16, 17]. Reflections are shifted within $2\theta = \pm 0.03^\circ$ relative to their position in pure $C\text{-Gd}_2\text{O}_3$. This is explained by the fact that all phases are solid solutions of oxides based on neighboring REE ions, i.e., Eu^{3+} , Gd^{3+} , and Tb^{3+} . In addition, the terbium ion in the oxide has an effective oxidation state of $\text{Tb}^{3.64+}$ in air [29], which corresponds to the mean oxidation state of the cations in compound $\text{Tb}_{11}\text{O}_{20}$. All reflections are broadened and there is a wide halo in the region of small diffraction angles, which indicates the small size of crystallites and the presence of an amorphous phase.

Sample 2 is obtained from sample 1 by successive annealing in an H_2 atmosphere for 2 h. The sample is comprised of the phase of solid solution $C\text{-Gd}_2\text{O}_3\text{:Tb}^{3+}, \text{Eu}^{3+}$ (1 mol %) and the impurity phases of tetragonal Tb_7O_{12} (two strong reflections at $2\theta = 61.719^\circ$ and 64.350° , space group $R\bar{3}$, ICSD-73822) and $\text{Gd}(\text{CO}_3)\text{OH}$ (one reflection at $2\theta = 61.908^\circ$) with the diffraction peak intensities noticeably higher than the background level. Other reflections cannot be probably resolved within the technique used, and some of the reflections overlap with the reference reflections of $C\text{-Gd}_2\text{O}_3$. The reflections have deviations with respect to the 2θ angles, since the solid solutions of three oxides of Eu^{3+} , Gd^{3+} , and Tb^{3+} have a bixbyite structure, which contains two types of posi-

Table 1. Results of processing the XPD data of the annealing products for the samples synthesized by the sol-gel method

Sample/annealing conditions	Compounds containing Tb^{3+} and Eu^{3+} ions	Cell parameter*, Å	CSR, nm			
			222	004	044	226
1. 1% Eu, Tb (700°C , air)	$C\text{-Gd}_2\text{O}_3$, $\text{Gd}(\text{OH})_3$, $\text{Gd}(\text{CO}_3)\text{OH}$	—	<30 nm			
2. 1% Eu, Tb (700°C , H_2)	$C\text{-Gd}_2\text{O}_3$, Tb_7O_{12} , $\text{Gd}(\text{CO}_3)\text{OH}$	10.8030(6)	34(3)	35(3)	37(3)	40(4)
3. 1% Eu, Tb (900°C , air)	$C\text{-Gd}_2\text{O}_3$, Tb_7O_{12} , $\text{TbO}_{1.81}$	10.8187(5)	33(3)	35(3)	36(3)	42(4)
4. 1% Eu, Tb (900°C , H_2)	$C\text{-Gd}_2\text{O}_3$	10.8083(2)	86(9)	87(9)	71(8)	54(5)
5. 1% Eu, Tb (1200°C , air)	$C\text{-Gd}_2\text{O}_3$, Tb_7O_{12}	10.8091(1)	—**			
6. 1% Eu, Tb (1200°C , H_2)	$B\text{-Gd}_2\text{O}_3$, Tb_7O_{12}	—	—			
7. 2.5% Eu, Tb (1200°C , air)	$C\text{-Gd}_2\text{O}_3$	10.8040(2)	120***	140***	100***	100***
8. 2.5% Eu, Tb (1200°C , H_2)	$C\text{-Gd}_2\text{O}_3$	10.7958(2)	170***	150***	—**	120***

*Reference cell parameters: $a = 10.81$ Å for Gd_2O_3 (ICSD-96207); 10.86 Å for Eu_2O_3 (JCPDS-34-392); and 10.76 Å for Tb_2O_3 (JCPDS-23-1418).

**Full widths at half maximum of the peaks are equal to the full widths at half maximum of the reference peaks of the Si standard. The CSR values cannot be calculated.

*** Full widths at half maximum of the peaks are close to the full widths at half maximum of the peaks of the Si standard. The CSR values are calculated approximately.

tions of REE cations in the unit cell, namely, eight ions in the centrosymmetric C_{3i} positions and twenty four ions in the noncentrosymmetric C_2 positions. Moreover, the distribution of elements over the positions depends on the ionic radius [30–34], on the temperature of synthesis or homogenizing annealing [14], and on the conditions of compound synthesis, which can be the sol-gel process [1, 22, 33], the hydrothermal method [3], the solid-phase sintering [34], etc. The CSR size determined by the Debye–Scherrer model is 36 ± 3 nm for the isometric shape of crystallites.

Sample 3, which is a sol-gel product annealed in air at 900°C for 1 h, contains the phase of cubic solid solution $C\text{-Gd}_2\text{O}_3\text{:Tb}^{3+},\text{Eu}^{3+}$ (1 mol %). In consequence of the fact that the sample was annealed in an air atmosphere with subsequent free cooling, the structure contains $\text{Tb}^{3.4+}$ ions, since seven reflections correspond to the trigonal Tb_7O_{12} phase (see Fig. 1), three reflections at $2\theta = 29.239^\circ$, 48.683° , and 57.804° correspond to the main reflections of the cubic $\text{TbO}_{1.81}$ phase that belongs to space group $Fm\bar{3}m$ (ICSD-28916). The presence of these phases does not contradict the thermography data [29], which indicate a change in the stoichiometry of terbium oxide and, consequently, a change in the effective oxidation state of terbium ions after heating in air. The established reflections of the oxide phases of $\text{Tb}^{3.4+}$ are located quite close to the reflections of the $C\text{-Gd}_2\text{O}_3$ phase and are partially overlapped with them, changing their reference intensity. This gives grounds to assume that semicoherent interfaces are formed between the phases, by analogy with compounds that have incommensurate sublattices [35, 36]. Moreover, impurity phases can be represented by polysynthetic twin layers of nanometer sizes.

Sample 4 synthesized from sample 3 by annealing at 900°C for 1 h in H_2 is comprised of one phase of solid solution $C\text{-Gd}_2\text{O}_3\text{:Tb}^{3+},\text{Eu}^{3+}$ (1 mol %). The Tb_7O_{12} phase is absent, since the Tb^{4+} ions in the oxide are reduced to Tb^{3+} in the H_2 atmosphere. The coherent scattering region is 36 ± 3 nm for sample 3, and increases to 86 ± 9 nm in the [222] and [004] directions, to 71 ± 8 nm in the [044] direction, and to 54 ± 5 nm in the [226] direction for sample 4.

Sample 5 was obtained by annealing a sol-gel product at 1200°C for 1 h and mainly contains the cubic phase of solid solution $C\text{-Gd}_2\text{O}_3\text{:Tb}^{3+},\text{Eu}^{3+}$ (1 mol %) with a coherent scattering region at the level of that for the reference micrometer-size indicates an increased degree of crystallinity. For pure $C\text{-Gd}_2\text{O}_3$, the cubic bixbyite lattice is a basic one lattice up to 1200°C [30]. However, this modification is a thermodynamically metastable modification according to the conclusions drawn in [37]. An impurity phase is found, four reflections of which are close to those of the Tb_7O_{12} phase.

Sample 6 obtained from sample 5 by annealing at 1200°C for 1 h in H_2 is comprised of the monoclinic $B\text{-Gd}_2\text{O}_3\text{:Tb}^{3+},\text{Eu}^{3+}$ (1 mol %) phase belonging to space group $C2/m$ and an impurity phase of trigonal Tb_7O_{12} (four reflections) that contains $\text{Tb}^{3.4+}$ cations. The appearance of the $B\text{-Gd}_2\text{O}_3\text{:Tb}^{3+},\text{Eu}^{3+}$ (1 mol %) phase after annealing in a reducing H_2 atmosphere at 1200°C is explained by the specific behavior of the stability of the cubic and monoclinic phases of REE oxides [29, 37, 38]. To check this feature, sample 6 was additionally annealed at 1200°C for 1 h in air (sample 9) and sample 5 was annealed at 1200°C in high-purity grade Ar for 1 h (sample 10). In both cases, phases of monoclinic $B\text{-Gd}_2\text{O}_3\text{:Tb}^{3+},\text{Eu}^{3+}$ (1 mol %) containing an impurity of the trigonal Tb_7O_{12} phase were obtained. Thus, polymorphic transition to the monoclinic phase occurs after annealing for 3 h in total. This confirms the well-known conclusion [37] that the cubic structure of sesquioxides of cerium group, including $C\text{-Gd}_2\text{O}_3$, is a metastable phase at low temperatures and can be converted into the monoclinic phase at elevated temperatures with a sufficient annealing time. The $C\text{-Gd}_2\text{O}_3$ lattice is a basic one lattice at a relatively low concentration of dopants. However, we have previously found that solid solutions of rare-earth oxides based on $C\text{-Gd}_2\text{O}_3$ can be stabilized by Eu^{3+} impurities in high concentrations [15].

To test the effect of an increased concentration of PL activators, samples 7 and 8 with Tb^{3+} and Eu^{3+} concentrations of 2.5 mol % each were synthesized. Both samples contain the phase of the cubic modification of $C\text{-Gd}_2\text{O}_3\text{:Tb}^{3+},\text{Eu}^{3+}$ (2.5 mol %) with CSR of 120 and 150 nm, respectively. The formation of the cubic modification of sample 7, which is a sol-gel product annealed in air at 1200°C for 1 h, and its retention after additional annealing in H_2 at 1200°C for 1 h are explained by the stabilizing effect of Eu^{3+} and Tb^{3+} ions. The resulting $C\text{-Gd}_2\text{O}_3$ matrix is a metastable phase in terms of thermodynamics [15, 37] and is probably stabilized by terbium sesquioxide (Tb^{3+}), which is thermodynamically stable in a cubic modification at these temperatures. The absence of the Tb_7O_{12} impurity phase and, consequently, Tb^{4+} cations is probably associated with the formation of stable $\text{Tb}^{3+}\text{-O}^{2-}\text{-Eu}^{3+}$ clusters due to exchange interactions with concentrations Eu^{3+} and Tb^{3+} ions above 1.5 mol %, as was established for the CaWO_4 matrix [19].

The IR spectra of the samples are shown in Fig. 2. With an increase in the annealing temperature in the range of $700\text{--}1200^\circ\text{C}$, dehydroxylation of the samples and a decrease in the content of carbonate ions occur, which is reflected in a decrease in the intensity of absorption bands of molecular water in the range of wavenumbers $1400\text{--}3600\text{ cm}^{-1}$, and absorption bands of O–H groups and asymmetric stretching vibrations of C–O groups at 1510 and 1400 cm^{-1} , respectively

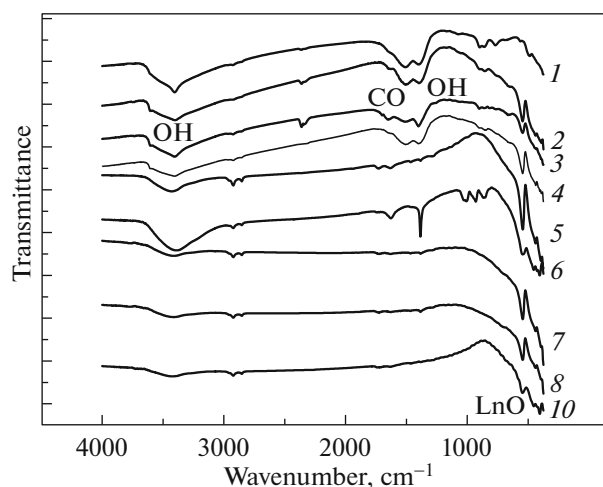


Fig. 2. Infrared spectra of samples 1–10.

[33]. The bands in the region of 390–600 cm^{-1} are related to stretching vibrations of Ln–O bonds in the C-Gd₂O₃ [39, 40], C-Eu₂O₃ [41], and C-Tb₂O₃ [42] sublattices and Ln–O bonds of the monoclinic lattice and impurity phases (sample 6). It is noteworthy that the absorption bands of O–H groups appear after annealing at high temperatures of 1200°C in an atmosphere of H₂ (sample 6), which is probably explained by the fact that the reduction of Tb⁴⁺ ions (or the reduction of an effective oxidation state of 3.64+ in the Tb₁₁O₂₂ matrix or 3.40+ in the Tb₇O₁₂ matrix to Tb³⁺). In this case, oxygen is released and forms adsorbed hydroxyl groups by reacting with H₂. A control experiment with additional annealing of sample 5 in an Ar

atmosphere showed the absence of O–H groups (sample 10).

The PL spectra normalized with respect to intensity are shown in Figs. 3a and 3b.

The spectra of the samples are given by histograms of the main PL band maxima (Fig. 3a), which give a clear idea of the change in the PL intensities from sample to sample. The real spectra of samples 1–5 are similar to the spectra of samples 7 and 8 (Fig. 3b) with different ratios of band intensities, which are given in Tables 2 and 3. Shifts of the band maxima along the radiation wavelength are noted, which is associated with a change in the crystal field in the coordination spheres of the PL activators. This may be a result of changing the real lattice structure (defectiveness) and redistributing the cations over the C₂ and C_{3i} states and over the surface C_s states.

The obtained results indicate that the intensity of emitted radiation in the reference bands of Tb³⁺ and Eu³⁺ ions increases with an increase in the annealing temperature. This is a result of dehydration of compounds and an increase in the degree of crystallinity of the samples. Moreover, the effect of dehydration in a multiphase system on the redistribution of the excitation energy over the bands can hardly be explained at the existing level of theoretical knowledge.

The analysis of the I_{612}/I_{595} ratio of the PL band intensities of Eu³⁺ ions, which arise from radiative transition ${}^5D_0 \rightarrow {}^7F_2$ at 612 nm and radiative transition ${}^5D_0 \rightarrow {}^7F_1$ at 595 nm, respectively, is a well grounded analysis of the redistribution of cations over the C₂ and C_{3i} sites. This ratio is proportional to the ratio of concentrations of Eu³⁺ ions in the indicated lattice positions and is called the “asymmetric ratio” (AR) [43, 44].

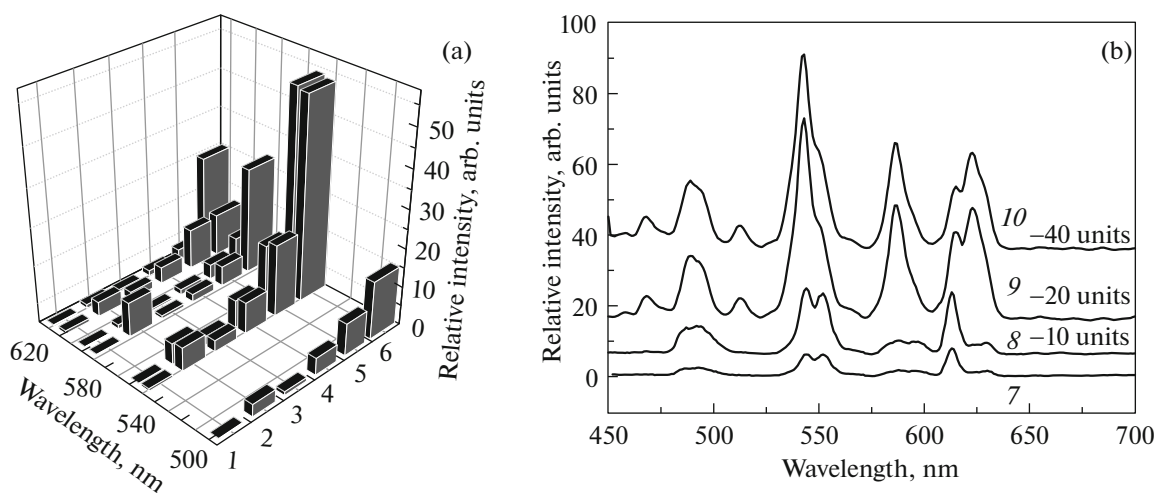


Fig. 3. (a) Photoluminescence spectra of samples 1–6 in the form of 3D histograms of the maxima of the main emission bands of Tb³⁺ ions at 487, 513, 542, 550, and 584 nm and Eu³⁺ ions at 595, 612, and 622 nm, and (b) general views of the spectra of samples 7–10; the spectra of samples 8, 9, and 10 are raised by 10, 20, and 40 intensity units, respectively.

Table 2. Intensities of the PL bands of the samples in relative units after the decomposition of the spectra into components

λ , nm	460	487	513	542	550	560*	584	596	612	622
Transition/ sample	$^5D_3 \rightarrow ^7F_3$	$^5D_4 \rightarrow ^7F_6$	$^5D_4 \rightarrow ^7F_6$	$^5D_4 \rightarrow ^7F_5$	$^5D_4 \rightarrow ^7F_5$		$^5D_4 \rightarrow ^7F_4$	$^5D_0 \rightarrow ^7F_1$	$^5D_0 \rightarrow ^7F_2$	$^5D_0 \rightarrow ^7F_2$
1	0.1	0.2	–	0.7	0.6	0.3	0.2	0.1	0.8	0.2
2	0.6	3	–	6	6	–	9	1	4	1
3	0.2	1	–	3	2	0.6	0.8	0.5	2	0.5
4	0.7	5	–	8	7	–	2	1.4	4	1.4
5	1.7	9	–	19	17	–	5	4	11	3
6	4.5	15/ (495 nm) 12	53	5	54/ (552 nm) 17	4	28	7	11	25
7	–	3	–	7	7	–	2	2	11	2
8	–	10	–	22	19	–	5	5	24	4
9	5	17	5	52	16	4	19/ (589 nm) 14	–	11	30
10	5	16/ (496 nm) 9	6	48	16	–	27	8	11	26

The second harmonic at $\lambda_{ex} = 280$ nm.

Table 3. Intensity ratios of the main emission bands of Eu^{3+} and Tb^{3+} ions for samples obtained under different annealing conditions with different concentrations of PL activators

Ratio $\lambda^*/$ sample/annealing conditions	610–614/ 594–596; AR	610–614/ 487–491	610–614/ 541–543	610–614/ 622–624	487–491/ 541–543	548–522/ 541–543	594–596/ 487–491	594–596/ 541–543	622–624/ 487–491	622–624/ 541–543
1. 1% Eu, Tb(700°C, air)	8	4	1.1	4	0.3	0.8	0.5	0.1	1	0.3
2. 1% Eu, Tb(700°C, H ₂)	3.5	1.2	0.6	3.8	0.5	0.9	0.3	0.2	0.3	0.2
3. 1% Eu, Tb(900°C, air)	4	2	0.7	4	0.3	0.8	0.5	0.2	0.5	0.2
4. 1% Eu, Tb(900°C, H ₂)	3	1	0.5	3.1	0.5	0.9	0.3	0.2	0.3	0.2
5. 1% Eu, Tb(1200°C, air)	2.8	1.2	0.6	3.5	0.5	0.9	0.4	0.2	0.4	0.2
6. 1% Eu, Tb(1200°C, H ₂)	1.5	0.7	2.2	0.4	3	5	0.5	1.5	1.6	5.0
7. 2.5% Eu, Tb(1200°C, air)	6	3.6	1.6	5.7	0.5	0.9	0.6	0.3	0.6	0.3
8. 2.5% Eu, Tb(1200°C, H ₂)	5	2.3	1.1	5.5	0.5	0.8	0.5	0.2	0.4	0.2
9. 1% Eu, Tb (no. 6, 1200°C, air)	1.3	1.1	0.4	0.6	0.3	0.3	1	0.3	1.7	0.6
10. 1% Eu, Tb (no. 5, 1200°C, Ar)	1.4	0.9	0.2	0.4	0.3	0.3	0.5	0.2	1.7	0.5

*Variation ranges in the position of the PL band maxima are indicated.

Sample 2 after annealing of sample 1 in H_2 is characterized by sharp increases in the intensity of the band of Tb^{3+} at 490 nm by a factor of 16, in the intensity of the superposition of bands (doublet [45]) at 542 and 550 nm by a factor of 18, and in the intensity of the band at 585 nm by a factor of 40. Moreover, the emission band of Eu^{3+} at 595 nm increases by an order of magnitude with an increase in the intensity of the band at 612 nm merely by a factor of 5. It is understandable that the Tb^{4+} ions reduced to Tb^{3+} are located preferably at the C_{3i} lattice sites. The concentration of Eu^{3+} ions increases predominantly in the C_{3i} sites because of transferring these ions into the bulk of the material with a decrease in the specific surface area of crystallites, in which they occupied the noncentrosymmetric C_s sites. Moreover, the probability of incorporating these ions into the C_{3i} sites with a smaller volume of the surrounding sphere is rather high in accordance with the following descending order of radii of the cations: $Gd^{3+} > Eu^{3+} > Tb^{3+}$ [27, 46]. The noted violation of the so-called “lanthanide contraction” of neighboring Eu^{3+} and Gd^{3+} ions has been recorded in the literature, and we have earlier observed it for solid solutions of oxides in the $(Gd_xY_{1-x})_2O_3:Eu^{3+}$ system [15]. This feature of Eu^{3+} ions was also found in the anomalous shift of the Raman band of Eu^{3+} ions in the region of 340–380 cm^{-1} for the series of lanthanides in the spectra of the corresponding cubic sesquioxides [47], which can be explained by an enhanced electron–phonon interaction. In particular, the PL excitation of Eu^{3+} ions occurs through electronic transitions ${}^5D_4 (Tb^{3+}) \rightarrow {}^5D_{1,2} (Eu^{3+})$. Energy is predominantly transferred along the C_{3i} sublattice within the energy of the ${}^5D_4 \rightarrow {}^7F_6$ transition (487 nm), since the lowest increase in the intensity of this band was found after annealing of the precursor, i.e., sample 1. The AR value naturally decreases substantially and practically reaches the equilibrium value for the bixbyite lattice ($AR_{eq} = 3$).

Annealing of the sol-gel product (sample 3) in air at 900°C leads to an increase in the emission of all radiative transitions in Tb^{3+} by a factor of 4–5 compared to sample 1, while the emission of the ${}^5D_0 \rightarrow {}^7F_1$ (595 nm) transition in the Eu^{3+} ion increases proportionally. The proportional distribution of energy over radiative transitions indicates that the distribution of PL activator Tb^{3+} over local cation sites is preserved and an increase in the radiation efficiency is associated with an increase in the degree of crystallinity of the sample. It should be noted that the annealing process is accompanied by a decrease in the concentration of Tb^{4+} ions due to reduction of them to Tb^{3+} with a decrease in the partial pressure of oxygen relative to its equilibrium value at a given temperature [29]. Excitation of the emission of the ${}^5D_0 \rightarrow {}^7F_2$ transition increases only by a factor of 2.5 and is probably associ-

ated with an increase in the crystallinity of the samples in comparison with sample 1 (see CSR, Table 1). In this case, the AR value decreases by a factor of 2, which indicates an increase in the concentration of Eu^{3+} ions in the C_{3i} lattice sites. This is a result of the transfer of some of these ions from the surface to the bulk of the material with a decrease in the specific surface area of crystallites. Moreover, the transfer of excitation energy of the emission band of Eu^{3+} at 612 nm and, to a lesser extent, of the band at 595 nm occurs within the energy of the ${}^5D_4 \rightarrow {}^7F_6$ transition of Tb^{3+} (487 nm), since the total emission energy of the doublet of bands at 542 and 550 nm increased by a factor of 8 with an increase in the emission energy of the band at 487 nm merely by a factor of 5. In this case, the ratio between the AR and the I_{612}/I_{487} intensities decreases proportionally by a factor of 2 in comparison with sample 1 at a constant I_{595}/I_{487} . The transfer of PL excitation of Tb^{3+} ions to Eu^{3+} ions has been noted earlier [1, 19].

Sample 4 obtained from sample 3 after annealing in H_2 is characterized by efficient reduction of Tb^{4+} to Tb^{3+} and a sharp increase in the degree of crystallinity (CSR increases, see Table 1). Accordingly, the intensity of all PL bands increases moderately (by a factor of 2–3). At the same time, relative increases in the emission intensities of the ${}^5D_4 \rightarrow {}^7F_6$ transitions (487 nm) by a factor of 4.5 and of the ${}^5D_4 \rightarrow {}^7F_5$ doublet by a factor of 5.7 in total are observed. A slightly larger increase in the emission intensity of the ${}^5D_0 \rightarrow {}^7F_1$ transition is associated with the transfer of Eu^{3+} ions from the C_s sites on the crystallite surface into the bulk of the material to the C_{3i} sites.

Annealing of a sol-gel product at 1200°C in air (sample 5) gives rise to a further increase in the concentration of Tb^{3+} ions [29] and a decrease in the specific surface area of crystallites relative to the results of annealing at 900°C (sample 3). According to this, the intensities of all emission bands increase by a factor of 5–7 for the most part. The emission intensity of the ${}^5D_4 \rightarrow {}^7F_6$ transition at 487 nm and the total intensity of the ${}^5D_4 \rightarrow {}^7F_5$ doublet transitions at 542 and 550 nm in Tb^{3+} ions show the largest increases by factors of 8 and 12, respectively. At the same time, the AR value decreases insignificantly and the I_{612}/I_{487} ratio slightly increases. The latter corresponds to the transfer of enhanced PL excitation from the Tb^{3+} activator to Eu^{3+} ions through the C_2 sublattice in addition to the excitation of emission due to $4f \rightarrow 4f$ transitions of Eu^{3+} ions. In actual fact, the I_{595}/I_{487} ratio slightly decreases (Table 2).

Sample 6 obtained from sample 5 after annealing in H_2 comprises a monoclinic phase based on the $B-Gd_2O_3$ matrix. A significant increase in the total intensity of the emission bands of Tb^{3+} at 487 and

550 nm is noted, which is naturally associated with the reduction of Tb^{4+} ions to Tb^{3+} ions that are effective PL site. In this case, the intensity of the emission band at 622 nm (taking into account shifts to the region of 622–624 nm) increases very strongly, which can be explained by the superposition of the ${}^5D_0 \rightarrow {}^7F_2$ radiative transitions of Eu^{3+} ions [48] (the low-energy component of the doublet) and the ${}^5D_4 \rightarrow {}^7F_3$ transitions of Tb^{3+} ions. The conversion of gadolinium sesquioxide into the monoclinic modification is a normal phenomenon at 1200°C [37]. In this case, the emission band of Eu^{3+} ions in the C_{3i} lattice sites at 595 nm is due to the presence of centrosymmetric sites in the lattice of trigonal Tb_7O_{12} . Consequently, the trigonal phase is doped with Eu^{3+} ions. It is noticeable that an unreferenced PL band appears at 513 nm in the spectrum of the obtained monoclinic phases, which is probably formed by doublet emission of the ${}^5D_4 \rightarrow {}^7F_6$ transition of the Tb^{3+} ion.

Sample 7 with an increased content of PL activators at a level of 2.5 mol %, which is the cubic modification of solid solution $C-Gd_2O_3:Tb^{3+},Eu^{3+}$ (2.5 mol %) of the bixbyite type, is formed as a result of annealing of a sol–gel product in air at 1200°C for 1 h. In this case, the intensities of the bands of Tb^{3+} at 487, 542, and 550 nm decrease by a factor of 2.5–3, the intensity of the PL band of Eu^{3+} ions at 596 nm increases by a factor of 5, and the intensity of the emission band at 612 nm remains the same relative to sample 5, which is also synthesized by annealing at 1200°C. These effects are associated with the onset of the well known effect of PL quenching of Tb^{3+} ions at concentrations of >1.5 mol % [19]. A relatively larger increase in the intensity of the emission band of the ${}^5D_0 \rightarrow {}^7F_1$ transition of Eu^{3+} ions at 596 nm in comparison with sample 5 is explained by a two-fold higher concentration of PL activators with a noticeable decrease in the degree of crystallinity of the sample due to an increase in the specific surface area of crystallites. This is associated with an increase in the concentration of Tb^{3+} ions in the surface states, which leads to the transfer of Eu^{3+} ions from the C_s surface states into the bulk of the material to the C_{3i} sites. These conclusions are based on the well known belief that the Tb^{3+} ion is an inhibitor of the growth of crystallites in a similar chemical system [1, 9]. Indeed, a decrease in the CSR is observed in sample 7 compared to sample 5 (see Table 1). Apparently, all additionally provided Eu^{3+} ions occupy the C_{3i} positions, since the intensity of the band at 612 nm remains at the level that was in sample 5. Subsequent annealing of sample 7 in H_2 for 1 h (sample 8) leads to increases in the emission band intensities of the ${}^5D_4 \rightarrow {}^7F_5$ transitions of Tb^{3+} at 542 and 550 nm and of Eu^{3+} at 612 nm by a factor of 2.0–2.5 relative to sample 5 with a lower activator concentration, reaching the maximum PL efficiency of both activators for the

cubic modification of a solid solution with the $C-Gd_2O_3:Tb^{3+},Eu^{3+}$ (2.5 mol %) composition.

The maximum intensities of the PL bands of Tb^{3+} at 487 and 542 nm are achieved in samples 6, 9, and 10, which consist of the monoclinic phase. Sample 10 is obtained by additional annealing of sample 5 in Ar for 1 h. The efficient photoluminescence is probably related to the fact that the cations coordinate seven O^{2-} ions, in the monoclinic modification [46], which contributes to the more efficient transfer of excitation energy to Tb^{3+} ions. For Eu^{3+} ions, the transition from the octahedral environment can lead to the transfer of excitation from the 5D_2 level of Eu^{3+} to the closely lying 5D_4 level of Tb^{3+} when the excitation energy of photons is high (280 nm). As a result, the intensity of the band of the monoclinic phase at 612 nm remains at the maximum level for the cubic phase. However, the band of the ${}^5D_0 \rightarrow {}^7F_1$ transition in Eu^{3+} at 595 nm has a slightly higher intensity. The presence of this band is associated with the impurity of the trigonal phase of solid solution $Tb_7O_{12}:Eu^{3+}(x)$ (space group $R\bar{3}$), in which half of the Tb^{3+} cations occupy the centrosymmetric C_{3i} positions. The spectra of the monoclinic phase (phases 6, 9, and 10) are characterized by a sharp decrease in band intensity ratio $(610-614)/(622-624) < 1$ relative to this parameter for cubic phases in the range from 3.5 to 5.7 (Table 3). This is explained by a decrease in the oxygen pressure relative to the equilibrium pressure at 1200°C for Tb_7O_{12} . However, this effect has been observed earlier in the synthesis of compound $B-Gd_2O_3:Eu^{3+}$ (1.6 mol %) [13] when the integrated intensity of the PL spectrum increased as in our case. Sample 6 annealed in an H_2 atmosphere is characterized by significant increases in band intensity ratios $(610-614)/(541-543)$, $(622-624)/(541-543)$, $(487-491)/(541-543)$, and $(548-552)/(541-543)$ compared to those for the samples of cubic modification C . This indicates the excitation energy in the emission doublet of the ${}^5D_0 \rightarrow {}^7F_2$ transition of the Eu^{3+} ion at 610 and 622 nm is mainly transferred through the high-energy component (541–543 nm) of the ${}^5D_4 \rightarrow {}^7F_5$ transition doublet of the Tb^{3+} ion. This is consistent with an increase in the $(548-552)/(541-543)$ emission intensity ratio, which generally indicates increased phonon–electron interactions in sample 6. Moreover, this occurs preferentially in the sublattice of noncentrosymmetric C_2 sites of the Tb^{3+} and Eu^{3+} cations, since the spatial symmetry of these sites is lowered. In actual fact, the $(610-614)/(541-543)$ band intensity ratio is 2.2 for the noncentrosymmetric C_2 sites, while the $(594-596)/(541-543)$ band intensity ratio equals 1.5 for the centrosymmetric C_{3i} sites.

4. CONCLUSIONS

Solid solutions $\text{Gd}_{2(1-x)}\text{Tb}_x\text{Eu}_x\text{O}_3$ are characterized by photoluminescent properties that are determined by the modification of the lattice of the Gd_2O_3 matrix (which can be either cubic or monoclinic), the concentrations of the Tb^{3+} and Eu^{3+} activators, the composition of impurity phases, and the distribution of activators over the centrosymmetric (C_{3i}) and non-centrosymmetric (C_2) cationic sites of the bixbyite lattice and over the C_s surface states. Phase transformations accompanied with dehydration, dehydroxylation, and decomposition of carbonates occur during the annealing of precursors, i.e., products $\text{Gd}_{2(1-x)}\text{Tb}_x\text{Eu}_x(\text{OH})_y(\text{CO}_3)_z \cdot n(\text{H}_2\text{O})$ ($x = 1 \text{ mol } \%$) of the sol–gel process in the temperature range of 700–1200°C. Solid solutions $\text{Gd}_2\text{O}_3:(\text{Tb}^{3+})_x(\text{Eu}^{3+})_x$ that are mainly formed contain microinclusions of lamellas of the $\text{Tb}_7\text{O}_{12}:\text{Eu}^{3+}$ phase. These microinclusions are eliminated after additional annealing in a hydrogen atmosphere as a result of the reduction of Tb^{4+} cations into Tb^{3+} cations. The photoluminescence of such products at $\lambda_{\text{ex}} = 280 \text{ nm}$ is characterized by the predominance of the emission efficiency of the bands of Tb^{3+} ions in the blue and green regions of the spectrum. The Tb^{3+} and Eu^{3+} photoluminescence activators preferably substitute Gd^{3+} ions in the C_{3i} positions, and the excitation energy of the emission of the ${}^5D_0 \rightarrow {}^7F_{1,2}$ transitions of Eu^{3+} ions is partially transferred from Tb^{3+} ions mainly along the C_{3i} sites of the sublattice, despite the fact that the concentration of Tb^{3+} and Eu^{3+} cations is less than 1.5 mol %. Thus, exchange interactions of activators also exist when their concentrations are 1 mol %. A change in the intensity of PL bands of activators and an increase in the number of Eu^{3+} cations in the C_{3i} positions correlate with a decrease in the specific surface area of crystallites (an increase in the degree of crystallinity of the samples). Regardless of the air/hydrogen/argon atmosphere, the annealing of the samples at 1200°C for 2 h or longer leads to a phase transition of the matrix into the monoclinic modification with a $\text{Tb}_7\text{O}_{12}:\text{Eu}^{3+}$ impurity, while the emission intensity of Tb^{3+} ions reaches very high relative values in the bands at 487 and 550 nm. At the same time, the excitation energy of emission from the band of Eu^{3+} cations at 596 nm is transferred owing to a decrease in the emission intensity of the high-energy band of the doublet of the ${}^5D_4 \rightarrow {}^7F_5$ transition of the Tb^{3+} ion at 542 nm.

Samples with an activator concentration of 2.5 mol % have a stable cubic modification of solid solution $C\text{-Gd}_2\text{O}_3:\text{Tb}^{3+},\text{Eu}^{3+}$ (2.5 mol %). The degree of crystallinity of the samples slightly decreases owing to the appearance of crystal growth inhibitors on the surface of crystallites, which are Tb^{3+} ions in the C_s surface states. A corresponding increase in the concentration

of Eu^{3+} ions in the bulk of crystallites, predominantly in the C_{3i} positions, leads to the practical equality of the intensities of the bands of Eu^{3+} ions at 612 nm and the bands of Tb^{3+} ions at 542 and 550 nm.

ACKNOWLEDGMENTS

We are grateful to I.V. Korol'kov for performing the X-ray diffraction phase analysis of powder samples.

FUNDING

This study was performed within the framework of State assignment for the Nikolaev Institute of Inorganic Chemistry, Siberian Branch, Russian Academy of Sciences, in the field of fundamental research.

CONFLICT OF INTEREST

The authors declare that they have no conflicts of interest.

REFERENCES

1. A. Garcia-Murillo, A. de J. Morales Ramirez, F. de J. Carrillo Romo, M. Garcia Hernandez, and M. A. Dominguez Crespo, *Mater. Lett.* **63**, 1631 (2009).
2. M. Ou, B. Muteleta, M. Martini, R. Bazzi, S. Roux, G. Ledoux, O. Tillement, and P. Perriat, *J. Colloid Interface Sci.* **333**, 684 (2009).
3. Z. Xu, J. Yang, Z. Hou, C. Li, C. Zhang, S. Huang, and J. Lin, *Mater. Res. Bull.* **44**, 1850 (2009).
4. B. Lu, Ji-G. Li, and Y. S. Lu, *Sci. Technol. Adv. Mater.* **14**, 064202 (2013).
5. C. J. Shilpa, N. Dhananjaya, H. Nagabhushana, S. C. Sharma, C. Shivakumara, K. H. Sudheerkumar, B. M. Nagabhushana, and R. P. S. Chakradhar, *Spectrochim. Acta, A* **128**, 730 (2014).
6. G. Schaak and J. A. Koningstein, *J. Opt. Soc. Am.* **60**, 1110 (1970).
7. Z. K. Heiba, L. Arda, and Y. S. Hascicek, *J. Appl. Crystallogr.* **38**, 306 (2005).
8. G. Blasse and B. C. Grabmaier, *Luminescent Materials* (Springer, Berlin, 1994).
9. P. R. Singh, K. Gupta, and A. Pandey, *World J. NanoSci. Eng.* **2**, 13 (2012).
10. N. Dhananjaya, H. Nfgabhushana, B. M. Nagabhushana, B. Rudraswamy, C. Shivakumara, and P. S. Chakradhar, *Bull. Mater. Sci.* **35**, 519 (2012).
11. P. Wellenius, E. R. Smith, P. C. Wu, H. O. Everitt, and J. F. Muth, *Phys. Status Solidi A* **207**, 1949 (2010).
12. M. Faucher and P. Caro, *Phys. Rev. B* **23**, 607 (1981).
13. D. K. Williams, B. Bihari, and B. M. Tissue, *J. Phys. Chem. B* **102**, 916 (1998).
14. V. V. Bakovets, S. V. Belaya, T. D. Pivovarova, I. P. Dolgovesova, I. V. Korolkov, O. V. Antonova, and M. I. Rakhmanova, *J. Lumin.* **215**, 116633 (2019).
15. V. V. Bakovets, T. D. Pivovarova, I. P. Dolgovesova, I. V. Korol'kov, O. V. Antonova, and S. I. Kozhemyachenko, *Russ. J. Gen. Chem.* **88**, 992 (2018).

16. V. V. Bakovets, L. N. Trushnikova, P. E. Plyusnin, I. V. Korolkov, I. P. Dolgovesova, T. D. Pivovarova, and S. A. Savintseva, *Russ. J. Gen. Chem.* **83**, 1808 (2013).
17. V. V. Bakovets, L. N. Trushnikova, I. V. Korolkov, P. E. Plyusnin, I. P. Dolgovesova, T. D. Pivovarova, and N. I. Alferova, *Russ. J. Gen. Chem.* **83**, 1 (2013).
18. T. A. Pomelova, V. V. Bakovets, I. V. Korol'kov, O. V. Antonova, and I. P. Dolgovesova, *Phys. Solid State* **56**, 2496 (2014).
19. M. Nazarov and D. Y. Noh, *J. Rare Earths* **28**, 1 (2010).
20. V. V. Bakovets, E. S. Zolotova, O. V. Antonova, I. V. Korol'kov, and I. V. Yushina, *Tech. Phys.* **61**, 1064 (2016).
21. V. V. Bakovets, E. S. Zolotova, O. V. Antonova, I. V. Korol'kov, and I. V. Yushina, *Tech. Phys.* **61**, 1868 (2016).
22. A. de J. M. Ramirez, A. Garcia Murillo, F. de J. C. Romoa, M. G. Hernandez, D. J. Viguera, G. Chaderyron, and D. Boyer, *Mater. Res. Bull.* **45**, 40 (2010).
23. N. V. Gaponenko, Y. V. Hluzd, G. K. Maliarevich, I. S. Molchan, G. E. Thompson, S. Dabboussi, H. Elhouichet, S. Y. Prislowski, and A. A. Lutich, *Mater. Lett.* **63**, 621 (2009).
24. Z. Yahiaoui, M. A. Hassairi, M. Dammak, E. Cavalli, and F. Mezzadri, *J. Lumin.* **194**, 96 (2018).
25. M. Zhao, Z. Zhao, L. Yang, L. Dong, A. Xia, S. Chang, Y. We, and Z. Liu, *J. Lumin.* **194**, 297 (2018).
26. D. Li, W. Qin, S. Liu, W. Pei, Z. Wang, P. Zhang, L. Wang, and L. Huang, *J. Alloys Comp.* **653**, 304 (2015).
27. B. Antic, J. Rogan, A. Kremenovic, A. S. Nikolic, M. Vucinic-Vasic, D. K. Bozanic, G. F. Goya, and Ph. Colomban, *Nanotechnology* **21**, 245702 (2010).
28. R. D. Shannon and C. T. Prewitt, *Acta Crystallogr., B* **26**, 1046 (1970).
29. M. A. Flores-Gonzalez, G. Ledoux, S. Roux, K. Lebbou, P. Perriat, and O. Tillement, *J. Solid State Chem.* **178**, 989 (2005).
30. Z. K. Heiba and L. Arda, *Cryst. Res. Technol.* **43**, 282 (2008).
31. M. Mitric, P. Onnerud, D. Rodic, R. Tellgren, A. Szytula, and M. L. J. Napljalo, *J. Phys. Chem. Solids* **54**, 967 (1993).
32. B. Antic, M. Mitric, and D. Rodic, *J. Phys.: Condens. Matter.* **9**, 365 (1997).
33. H. Guoa, X. Yangb, T. Xiaob, W. Zhanga, L. Loub, and J. Mugnier, *Appl. Surf. Sci.* **230**, 215 (2004).
34. M. V. Belobeletskaya, N. I. Steblevskaya, and M. A. Medkov, *Vestn. DVO RAN* **56**, 33 (2013).
35. P. A. Cox, *The Electronic Structure and Chemistry of Solids* (Oxford Science, Oxford, 1987).
36. A. V. Sotnikov, V. V. Bakovets, E. V. Korotaev, S. V. Trubina, and V. I. Zaikovskii, *Mater. Res. Bull.* **131**, 110963 (2020).
37. P. P. Fedorov, M. V. Nazarkin, and R. M. Zaklyukin, *Crystallogr. Rep.* **47**, 281 (2002).
38. C. L. Luyer, A. Garcia Murillo, E. Bernstein, and J. Mugnier, *J. Raman Spectrosc.* **34**, 234 (2003).
39. D. B. Faithful, S. M. Johnson, and I. McColm, *Rev. Chim. Miner.* **10**, 291 (1973).
40. A. Garcia-Murillo, C. L. Luyer, C. Dujardin, C. Pedrini, and J. Mugnier, *Opt. Mater.* **16**, 39 (2001).
41. N. T. Mcdevitt and A. D. Davison, *J. Opt. Soc. Am.* **56**, 636 (1966).
42. M. W. Urban and B. C. Cornilsen, *J. Phys. Chem. Solids* **48**, 475 (1987).
43. H. S. Yoo, W. B. Im, S. W. Kim, B. H. Kwon, and D. Y. Jeon, *J. Lumin.* **130**, 153 (2010).
44. R. M. Krsmanovic, Z. Antic, M. G. Nikolic, M. Mitric, and M. D. Dramicanin, *Ceram. Int.* **37**, 525 (2011).
45. X. Gao, C. Li, S. Li, H. Zhang, Z. Li, Y. Hong, and J. Sun, *J. Lumin.* **190**, 457 (2017).
46. F. X. Zhang, M. Lang, W. Wang, U. Becker, and R. C. Ewing, *Phys. Rev. B* **78**, 064114 (2008).
47. N. Dilawar, S. Mehrotra, D. Varandani, B. V. Kumaraswamy, S. K. Haldar, and A. K. Bandyopadhyay, *Mater. Character.* **59**, 462 (2008).
48. S. V. Mahajan and J. H. Dickerson, *Nanotechnology* **18**, 325605 (2007).

Translated by O. Kadkin